Applied Materials Today 38 (2024) 102226

Contents lists available at ScienceDirect

Applied Materials Today

journal homepage: www.elsevier.com/locate/apmt

Hydrolysis of biobased stereocomplex polylactide: Polymorphism dependent crystals degradation and evolution of three-phase crystalline composition

Qi Chen [a,b], Ece Sogut [a], Rafael Auras [c], Jacob Judas Kain Kirkensgaard [d,e], Ilke Uysal-Unalan [a,b,*]

[a] Department of Food Science, Aarhus University, Agro Food Park 48, 8200, Aarhus N, Denmark
[b] CiFOOD – Center for Innovative Food Research, Aarhus University, Agro Food Park 48, 8200, Aarhus N, Denmark
[c] School of Packaging, Michigan State University, East Lansing, MI, 48824-1223, USA
[d] Department of Food Science, University of Copenhagen, 1958 Frederiksberg C, Denmark
[e] Niels Bohr Institute, University of Copenhagen, 2100 Copenhagen Ø, Denmark

ARTICLE INFO

Keywords:
Biodegradable
Bioplastic
Lactide
Rigid amorphous fraction
Structure-property relationship

ABSTRACT

The hydrolytic degradation behavior of stereocomplex polylactide (SCPLA) with distinct polymorphisms (*α, α′*, SC) and SC fractions (the ratio of SC crystallinity to total crystallinity) was first investigated in the present study. The evolution of three-phase crystalline compositions was quantified using modulated differential scanning calorimetry. Hydrolytic degradation commenced in the mobile amorphous fraction (MAF), while both the crystal (CF) and rigid amorphous fraction (RAF) began degradation on Day 3. By the 26th day, the MAF was consumed entirely, followed by the CF and RAF degraded at similar rates, primarily through the cleavage of chains with free ends on the folding surface of the remaining lamella. This work further discussed the influence of polymorphism on homochiral (HC) and SC crystal degradation during hydrolysis. Given racemic helices' participation in SC crystallization, SC-crystal lamellae may possess a higher number of amorphous chains with free ends than HC-crystals. This attribute could account for the faster degradation of HC-crystals in samples with a higher SC fraction.

1. Introduction

Polylactide (PLA) is a biobased polyester with ester groups susceptible to hydrolysis, leading to PLA degradation under humid conditions [1,2]. While this characteristic poses challenges to the storage [3] and processing of PLA, [4] also presents opportunities by offering sustainable attributes applicable in packaging industries and biomedical domains due to its commendable biocompatibility [5,6]. The hydrolytic degradation of PLA proceeds via water diffusion into the matrix, resulting in chain cleavage into PLA oligomers. The resulting oligomers, rich in carboxyl and hydroxyl end groups, enhance the hydrophilicity of the system, facilitating water attraction and creating an acidic environment for autocatalytic hydrolysis [7]. On the other hand, as a semicrystalline polymer, the crystalline regions of PLA play a pivotal role in its degradation behavior. A higher crystallinity can inhibit water diffusion, enhancing hydrolytic resistance [8]. However, other works indicate that end groups accumulated on the folding surface of crystal lamellae, intensifying the autocatalytic hydrolysis, thereby inducing greater degradation with increased crystallinity [9-12]. The recent discovery of stereocomplex PLA (SCPLA), with an SC-crystal having a melting temperature 50 °C higher than HC crystals, grants PLA-based materials exceptional properties [13-16], including enhanced hydrolytic resistance [17,18]. Tsuji has undertaken a series of works comparing the degradation behavior of PLA with *α* and SC-crystal forms [12,17,19,20]. However, investigations into the degradation behavior of individual SCPLA across different crystal forms or polymorphisms remain scarce but are crucial for designing SCPLA-based materials for practical applications.

The degradation process of semicrystalline polymers is initiated by the random hydrolytic scission of ester bonds in the amorphous regions, given their primary susceptibility to water diffusion with higher free volume than the crystalline regions [2]. Recent works, however, have

* Corresponding author at: Department of Food Science, Aarhus University, Agro Food Park 48, 8200 Aarhus N, Denmark.
E-mail address: iuu@food.au.dk (I. Uysal-Unalan).

https://doi.org/10.1016/j.apmt.2024.102226
Received 12 September 2023; Received in revised form 16 April 2024; Accepted 1 May 2024

also reported the importance of interfacial amorphous regions - referred to as rigid amorphous regions (RAF) - between the amorphous and crystalline regions [21-23] on the hydrolytic degradation behavior [24]. The RAF consists of chains with free ends, tie molecules, and folding chains that hold different conformations compared to the random coil chains in the mobile amorphous regions (MAF) [21,25]. Consequently, RAF exhibits a higher free volume than MAF [26,27], rendering it more susceptible to water diffusion [24,28]. Moreover, given the enrichment in free ends, chains in RAF are rich in the carboxyl groups and ester groups in end chains, which are more easily hydrolyzed [29]. The three-phase crystalline composition's evolution has yet to be quantified [24] since comprehending the three-phase crystalline composition evolution is crucial for designing semicrystalline polymers with tailor resistance to hydrolysis.

In the present work, we investigated the hydrolytic degradation of SCPLA. The three-phase crystalline compositions were quantified, and the influence of polymorphism (α, α', and SC-crystal) on hydrolytic degradation for 90 days were examined. A layered double hydroxide (LDH) filler was introduced into SCPLA, serving as a comparative platform and validating the observed correlation between degradation and structure in SCPLA nanocomposites. LDH, with its brucite-like layered structure, is defined by the chemical formula $[M^{2+}_{1-x}M^{3+}_{x}(OH)_2]^{x+}\cdot A_{x/n}{}^{n-}\cdot mH_2O$, where M^{2+} and M^{3+} represent metal cations, and A^{n-} denotes exchangeable interlayer anions [30]. Being biocompatible and low cytotoxic clay, incorporating LDH into a PLA-based matrix could render promising applications in food packaging [31] and biomedical fields [31]. Degradation characteristics of PLA through hydrolysis in the presence of LDH and consequent impact on material properties are essential to determine. Several works have focused on the effect of LDH on PLA hydrolytic degradation at high loading (> 1 wt%). For instance, Oyarzabal et al. [32] studied the impact of 5 wt% LDH on PLA hydrolysis. It was concluded that the barrier effect of LDH might retard oligomer diffusion in the early stage of degradation, which catalyzes the degradation of PLA in the later stage of hydrolysis. Iozzino et al. [33] found that 3 wt% LDH loading could slow down the rate of molecular weight reduction during hydrolysis of PLA. However, the effect of LDH on SCPLA hydrolysis, particularly, at low LDH loading ($\leq$ 1 wt%) has not yet been investigated, even though such low content of LDH ($\leq$ 1 wt%) has demonstrated a significant effect on crystallization and barrier properties of SCPLA in previous works [30,34]. More research is needed to identify the factors and mechanisms that are associated with PLA/LDH degradation. Often this knowledge provides flexibility in controlling hydrolysis thus customizing the design of composite materials specific to their application.

2. Experimental section

2.1. Raw materials

PLLA, brand name Luminy® L130, with d-lactide content < 1 %, and PDLA, brand name Luminy® D120, with l-lactide content < 1 % were purchased from TotalEnergies Corbion (Gorinchem, Netherlands). LDH, trade name DHT-4A, chemically represented as $Mg_{4.3}Al_2(OH)_{12.6}CO_3\cdot mH_2O$, and containing less than 4 % fatty acid modification, was generously provided by Kisuma Chemicals (Veendam, Netherlands).

2.2. Film preparation

Pellets of PLLA and PDLA were mixed and fed into a Process 11 Parallel Twin-Screw Extruder with a 40/1 L/D ratio (Thermo Fisher Scientific, Massachusetts, USA) to produce pellet-form SCPLA blends (with a PLLA/PDLA weight ratio of 1:1). The SCPLA/LDH composites containing 0.5wt% LDH were prepared by feeding LDH powder with PLLA and PDLA pellets and then extruding the blend. The temperature profile of the extruder, from feeder to die, was set as 180, 220, 220, 230, 230, 240, 240, and 230 °C, and the screw speed was established at 100 rpm. The pellets of extruded neat SCPLA and SCPLA/LDH composites were subsequently compression molded utilizing a YLJ-HP300 heat press (MTI Corporation, California, USA) at 225 °C and 10 MPa for 5 min, a temperature higher than the melting temperature of SC-crystal [18]. The produced films were immediately pressed between two stainless steel sheets at room temperature, with a top weight of 1 kg. The films were further treated by compression molding at 80, 140, and 200 °C and 10 MPa for 30 min to produce annealed films with various polymorphisms. Specifically, crystallization during annealing at 80 °C results in the formation of α'-crystal, while annealing at 140 °C leads to generation of α-crystal [34]. Crystallization at 200 °C produces exclusive SC-crystal because such temperature is higher than the melting temperature of HC-crystal [18]. Films treated solely at 225 °C for 5 min were denoted as T_{225}, and films that underwent the additional treatment at 80, 140, and 200 °C for 30 min were labeled as T_{80}, T_{140}, and T_{200}, respectively.

2.3. Hydrolysis experiments

The hydrolysis test was derived from ASTM D4754–18 (34) and was carried out under unbuffered conditions in water at 60 °C for 90 days [35]. The hydrolysis procedure involved using a 4 mL glass vial equipped with a Teflon-lined cap. For both neat SCPLA and SCPLA/LDH composite, two rectangular film pieces from each treatment in dimensions 0.5 cm × 2 cm were cut and then placed in the vial containing 3 mL of Milli-Q water for the experimental setup. For each treatment, 3 vials containing 2 film pieces each were prepared. One piece from each vial (3 replicated for each film treatment) was collected at predetermined time points throughout the hydrolysis experiment, Day 0 (before hydrolysis), and Day 1, 3, 7, 14, 26, 40, 60, and 90.

2.4. Modulated differential scanning calorimetry

Modulated Differential Scanning Calorimetry (MDSC) was utilized to study the three-phase crystalline composition of the annealed films using a Q2000 instrument (TA Instruments, New Castle, USA). The measurements were conducted employing a modulation amplitude of ±0.318 °C, a period of 60 s, and a heating rate of 2 °C/min. Calibration of the instrument was conducted using indium and sapphire standards.

2.5. Small- and Wide-Angle X-ray scattering

The polymorphism and crystalline structure of the annealed SCPLA and corresponding LDH composite films were examined using Small- and Wide-Angle X-ray Scattering (SWAXS), facilitated through a NanoinXider (λ = 0.154 nm, Xenocs, Sassenage, France) operating at 50 kV, 0.6 mA, and a beam size of 800 μm within a q range from 0.01 to 4 $Å^{-1}$.

3. Results and discussions

Table 1 summarizes the melting temperatures and crystallinities of HC and SC in the SCPLA and SCPLA/LDH composites before the hydrolysis experiments. A clear relationship was identified between the annealing temperature and the generated polymorphism, evidenced by the WAXS pattern in Fig. 1S of the supplementary materials. Annealing at 225 °C (T_{225}) and 200 °C (T_{200}) produced exclusive SC-crystals, as the temperature is too high for HC-crystal to develop. The α-crystals were produced at an annealing temperature of 140 °C (T_{140}), whereas α'-crystals were derived from annealing at 80 °C (T_{80}), indicated by the shift in the diffraction peak at 16.6° and 19.0° and the disappearance of diffraction peaks at 14.8° [36]. This is aligned with the experiment observations that α'-crystals preferentially developed at a crystallization temperature lower than 120 °C [37,38]. Besides the polymorphism, it is essential to note the variation in the SC fraction present in T_{140} and T_{80},

Table 1
HC ($T_{m,\ HC}$) and SC ($T_{m,\ SC}$) melting temperatures, HC ($X_{c,\ HC}$) and SC ($X_{c,\ SC}$) crystallinities, total crystallinity (X_c) and SC fraction (ratio of $X_{c,\ SC}$ to sum of $X_{c,\ HC}$ and $X_{c,\ SC}$) of SCPLA and SCPLA/LDH composites films before hydrolysis degradation.

Sample	Annealing temperature (°C)	$T_{m,\ HC}$ (°C)[a]	$T_{m,\ SC}$ (°C)[a]	$X_{c,\ HC}$ (%)[b]	$X_{c,\ SC}$ (%)[b]	Total X_c (%)[b]	SC fraction (%)[b]
SCPLA	225	173.2 ± 0.3	224.1 ± 0.2	0	4.1	4.1	100
	200	172.2 ± 1.1	225.9 ± 0.6	0	35.6	35.6	100
	140	175.0 ± 0.3	225.0 ± 0.2	25.0	9.1	34.1	26.6
	80	173.8 ± 0.3	225.4 ± 0.1	17.7	14.3	32.0	44.6
SCPLA/LDH	225	172.8 ± 0.3	222.7 ± 0.3	0	5.3	5.3	100
	200	172.1 ± 0.5	224.2 ± 0.5	0	29.2	29.2	100
	140	174.0 ± 0.2	223.6 ± 0.2	20.1	10.0	30.1	33.3
	80	173.0 ± 0.3	222.3 ± 0.2	16.4	12.1	28.5	42.4

[a] T_m are reported as average of three replicates with ± standard deviation.
[b] Determined via WAXS by the ratio of the area of the crystalline peaks to the total area of the diffraction pattern. The crystalline peak areas were obtained by subtracting the amorphous halo from the total peak areas [39].

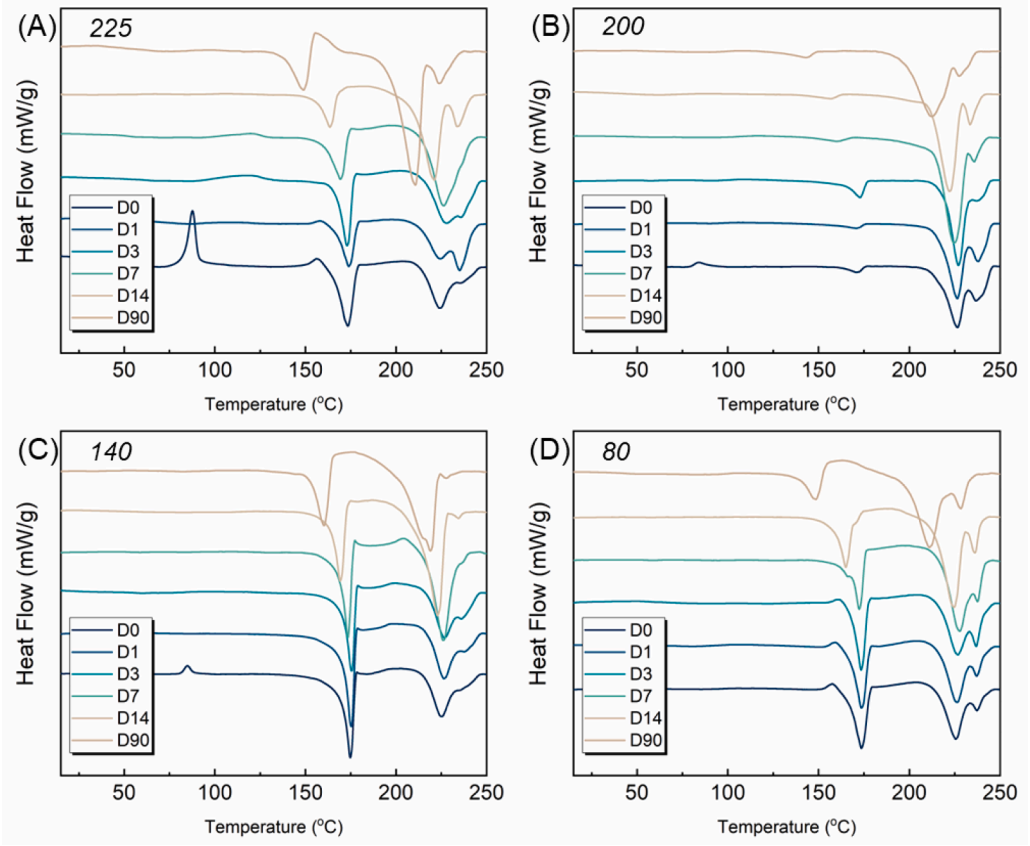

Fig. 1. DSC traces of SCPLA prepared from annealing at (A) 225 °C, (B) 200 °C, (C) 140 °C, and (D) 80 °C during hydrolytic degradation.

where a higher SC fraction was obtained in T_{80} samples probably due to the higher rate of SC-crystallization at 80 °C than 140 °C. A minimal alteration in the SC fraction was observed in the SCPLA with the addition of 0.5 wt% LDH. This finding deviates from previous works where LDH demonstrated selective enhancement in SC crystallization [30]. A plausible explanation for this discrepancy could be the slower cooling procedure employed in the current study after the thermocompression. This procedure potentially facilitated a higher development of SC crystallization during cooling, as seen in the exceptional SC development in the SCPLA at T_{80} and T_{140}, thereby diminishing the selective SC nucleation effect associated with LDH. The similarity in polymorphism and SC fraction between SCPLA and SCPLA/LDH provides opportunities to explore the influence of LDH on the hydrolysis of SCPLA and testify to the observed mechanism in both neat and LDH-filled SCPLA systems.

Upon hydrolysis, Fig. 1 provides selective DSC traces of SCPLA up to Day 90. The corresponding DSC traces of SCPLA/LDH composites can be found in Fig. 2S. On Day 0, the samples annealed at 225 °C (T_{225}) exhibited pronounced cold crystallization peaks, primarily due to their low initial crystallinity, which enabled crystallization during DSC scanning. In contrast, the cold crystallization peaks were minimal or negligible for the remaining samples (T_{200}, T_{140}, and T_{80}), owing to their high initial crystallinity, as seen in Table 1. As hydrolysis progresses, these cold crystallization peaks have diminished quickly since Day 1, probably due to the crystallization occurring during water immersion at 60 °C (above the glass transition temperature) [11,40]. Subsequently, there is a considerable decrease in both HC and SC melting temperatures ($T_{m,\ HC}$ and $T_{m,\ SC}$). The rate and extent of this decrease varied and are investigated closely in the later sections. The reduction in the $T_{m,\ HC,}$ and $T_{m,\ SC}$ could be ascribed to the decreasing lamellar thickness due to the hydrolysis of crystals [10,41]. This can be generally observed during the latter stages of hydrolysis, following the degradation of amorphous regions [42], detailed in the later section. Two distinct melting

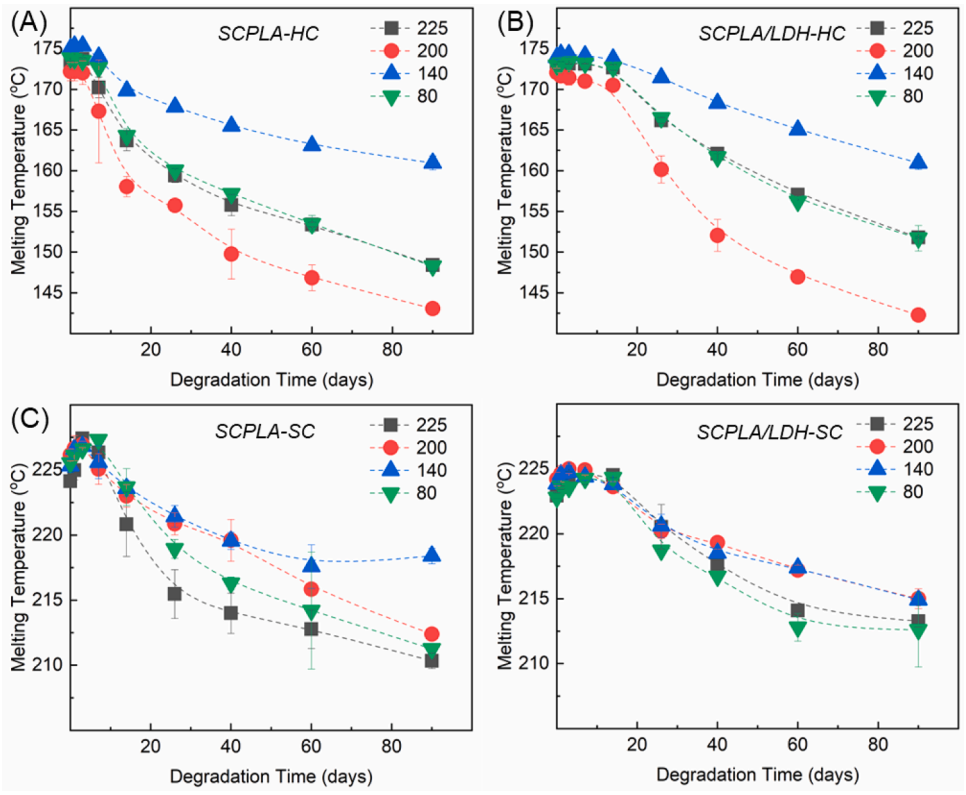

Fig. 2. Melting temperatures of HC (A-B) and SC-crystals (C-D) of SCPLA and SCPLA/LDH prepared from annealing at different temperatures (as marked in legend) during hydrolytic degradation.

temperatures were identified for the SC-crystals. Given that the WAXS pattern (Fig. 1S) did not display any diffractions other than those corresponding to SC-crystals, it can be deduced that the higher SC melting peak may correspond to the formation of thicker lamellar crystals, which can result from the recrystallization or annealing processes occurring during the DSC scanning [24].

To foster an understanding of the variation in T_m decrease during hydrolysis, Fig. 2 provides an evolution of $T_{m,\ HC}$ and $T_{m,\ SC}$ on various days of hydrolysis. In general, both $T_{m,\ HC}$ and $T_{m,\ SC}$ followed a downward trend over the hydrolysis, attributing to the degradation of crystals as mentioned above. Interestingly, this T_m reduction was not observed within the first three days, implying that degradation during the first three days predominantly occurred within amorphous regions rather than within the crystals. Another observation is the increase of $T_{m,\ SC}$ during the first three days (Fig. 2C and D), which might be ascribed to the post-SC crystallization taking place during water immersion at 60 °C, where the plasticized chain with higher mobility can crystallize into crystals with higher lamellae thickness [10]. Compared with SCPLA, SCPLA/LDH composites (Fig. 2B and D) displayed slower changes in both $T_{m,\ HC}$ and $T_{m,\ SC}$, indicating that LDH may inhibit not only the crystallization process (up to Day 3) but also the degradation process (after Day 3). It is noted that a higher amount of LDH ($\geq$ 1 wt%) has been found to facilitate the degradation of PLA by its metal ions; [43-45] therefore, such observed inhibition effect of LDH on SCPLA degradation might be associated with its lower loading level (0.5 wt%) in the present study. Furthermore, a correlation was evident between the reduction in $T_{m,\ HC,}$ and polymorphism (Fig. 2A and B). To be specific, HC-crystals in T_{140} samples with α + SC polymorphism exhibited superior resistance to hydrolysis among other polymorphisms. On the other hand, HC-crystals in T_{200} samples with exclusive SC polymorphism displayed the least hydrolytic resistance. The possible mechanism is discussed in a later section with more details on the structural development during the hydrolysis.

Before elaborating on the different trends of $T_{m,\ HC,}$ and $T_{m,\ SC}$ across the hydrolysis experiments, it is crucial to understand the structural changes of materials, particularly the changes in crystalline and amorphous fractions. The melting enthalpies of both SCPLA and SCPLA/LDH samples during hydrolysis are summarized in Fig. 3A and B. It reveals that the total enthalpies, representing the sum of HC and SC enthalpies, experienced a rise on 90 days of hydrolysis as compared to them before hydrolysis. This crystallinity increase can also be verified by the WAXS patterns of samples before and after hydrolysis in Fig. 3S, which also demonstrated that the T_{80} samples still maintained the α' + SC-crystal polymorphism after hydrolysis for 90 days. While the increase in total enthalpy corresponds to the increase in crystallinity, it should be noted that crystallinity is the numerical weight or volume ratio of the crystal region to the amorphous region. Therefore, total enthalpy increase can be ascribed to the combined consequence of crystallization or degradation of the amorphous region during the hydrolysis. Remarkably, unlike the changes in T_m (Fig. 2), such increases in total enthalpy primarily ceased after Day 26. The minimal changes in enthalpy after Day 26 but the continued changes in T_m (Fig. 2) suggest the absence of amorphous regions and the degradation may solely occur within the crystal structures after Day 26. Compared to SCPLA, the SCPLA/LDH demonstrated slower changes and reduced final enthalpy values, suggesting an inhibition effect of LDH at low content (0.5 wt%) on both degradation and crystallization.

Based on the observations drawn from the changes in T_m and enthalpy during the hydrolysis, it can be concluded that degradation during Day 0 to 3 occurred exclusively in the amorphous regions, causing increases in crystallinities. From Day 3 to Day 26, degradation took place in both the amorphous and crystalline regions, which led to the continued increase in crystallinity but a decrease in lamellae thickness (as indicated by T_m). From Day 26 onwards, only the crystal structure was subjected to degradation, and is discussed in later sections. This sequence of structural evolution is illustrated in Fig. 3C The

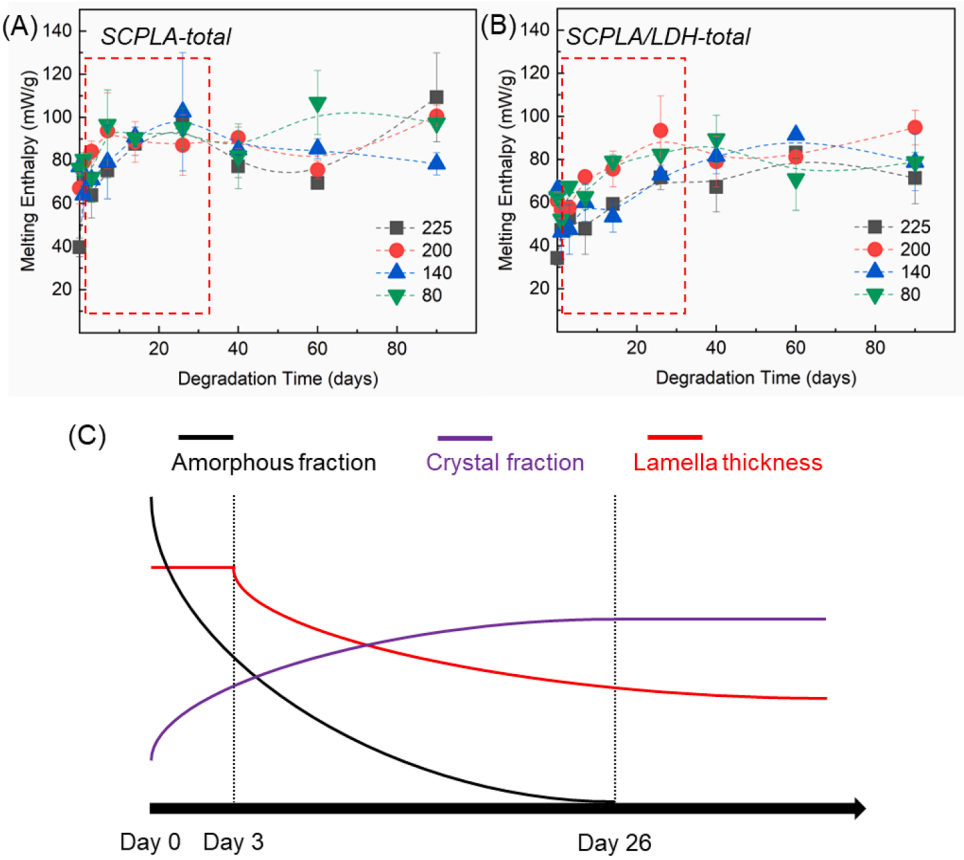

Fig. 3. Total melting enthalpies (melting enthalpies of HC-crystal + SC-crystal) of (A) SCPLA and (B) SCPLA/LDH prepared from annealing at different temperatures (as marked in legend) during hydrolytic degradation. (C) Schematic diagram of amorphous, crystalline fraction, and lamella thickness evolution during hydrolytic degradation.

variations in lamellar thickness during the hydrolysis process are further verified by the SAXS patterns shown in Fig. 4, where the shift of peaks to lower q values was only observed after Day 3. This shift is indicative of an increase in long spacing, which resulted from the reduction in lamellar thickness and expanded spacing between neighboring lamellas. Noted that the T_{80} samples exhibited less pronounced peaks, attributed to the conformational disorder [34]. However, it still needs to be made clear how crystallization proceeded during hydrolysis. Meanwhile, an interesting observation is that while the lamellar thickness (T_m) of the crystal diminished due to degradation within the crystal structure, the crystal enthalpies maintained a constant level after Day 26, as summarized by the evolution of crystal fraction (CF), amorphous fraction and lamellae thickness in Fig. 3C. Those questions will be discussed in the following section.

To understand the crystallization progress and lamellar thickness changes during hydrolysis, the MAF and RAF were estimated based on methods described in previous work [30]. Briefly, the MAF can be calculated by the ratio of the heat capacity change of a sample at the glass transition to the heat capacity change of the fully amorphous sample. RAF can be estimated from the equation of RAF = 1 – CF – MAF [30]. Fig. 5 presents the progression of MAF and RAF up to Day 26. The 90-day evolution of MAF and RAF is presented in Fig. 4S. Fig. 5A and B depict that the MAF quickly dropped in the initial three days. This can be attributed to the combined effect of amorphous region degradation and water-facilitated crystallization at 60 °C. Simultaneously, the RAF's evolution, demonstrated in Figs. 5C and 4D, experienced a sharp increase until Day 3. This increase in RAF appeared to cease after Day 3, while MAF continued to decrease at a slower rate. The RAF represents the interface between the crystal lamellae and the MAF region or neighboring lamellae; the rise in RAF is believed to be associated with the crystallization process. This suggests that the crystallization stopped after Day 3. Therefore, the continued decrease in MAF (Fig. 5A and B) and the increase in crystallinity (Fig. 3A and B) observed from Day 3 to Day 26 were attributed solely to the degradation of the MAF rather than crystallization.

The three-phase crystalline composition evolution can be summarized in Fig. 6A. Between Day 0 and Day 3, degradation and crystallization of amorphous regions took place concurrently, leading to an increase in enthalpies (Fig. 3A and B), a decrease in MAF (Fig. 5A and B), and an increase in RAF (Fig. 5C and D). From Day 3 to Day 26, crystallization ceased. Still, degradation occurred in both the crystal and amorphous regions. However, the amorphous regions degraded more quickly, resulting in a decrease in T_m (Fig. 2), an increase in enthalpies (Fig. 3A and B), and a slower decrease in MAF than that in Day 0–3 (Fig. 5A and B). This deceleration of MAF may be attributed to the remaining amorphous regions being protected by the crystal regions against water diffusion. After Day 26, all MAF regions had degraded, and only the crystal and RAF regions continued to degrade, leading to a sustained decrease in T_m (Fig. 2) but constant levels of enthalpies (Fig. 3A and B) and RAF (Fig. 5C and D). Such consistent RAF and enthalpy levels after Day 26 might indicate that the crystal lamellae and its associated RAF degrade at similar rates, otherwise causing changes in RAF or enthalpies. Fig. 6B selectively shows the typical photos of T_{225} samples captured during the hydrolysis, and photos for other samples are shown in Fig. 5S. All samples remained in their original shape and dimension in the vial till Day 90 while getting too brittle to be washed out on Day 7. Therefore, the hydrolysis degradation of samples in the present study adopts a bulk erosion mechanism [46,47], which can also be confirmed by the unchanged film thickness during hydrolysis up to Day 7 in Table 1S. Importantly, the bulk degradation of the films during

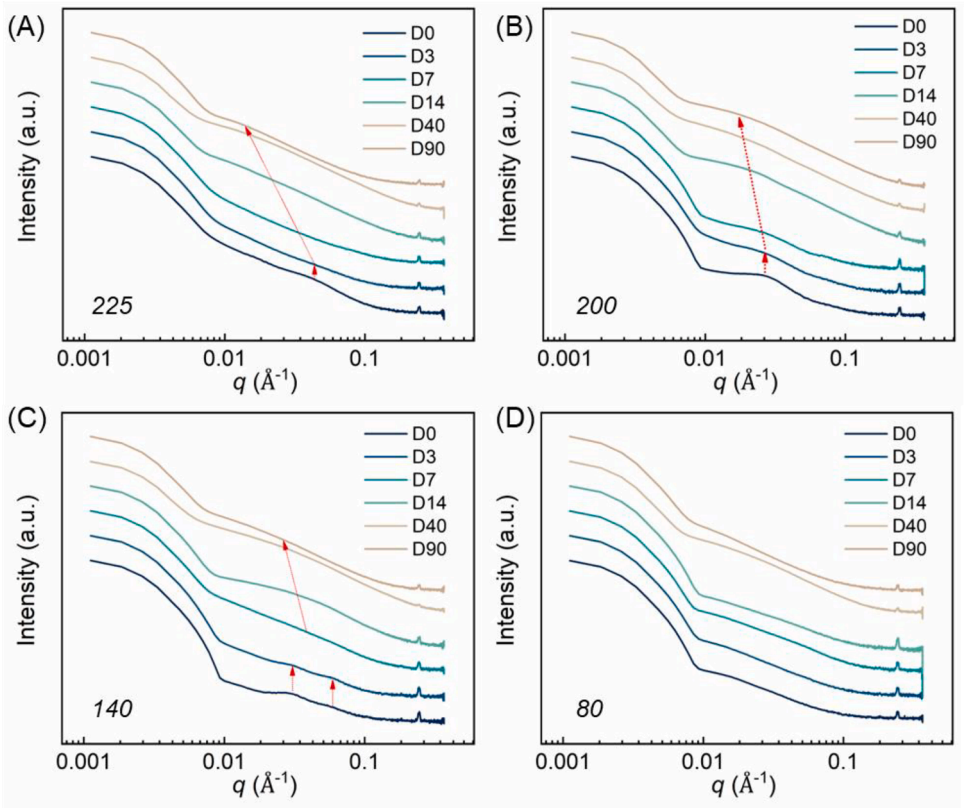

Fig. 4. SAXS patterns of SCPLA obtained from annealing at (A)225 °C, (B) 200 °C, (C) 140 °C, and (D) 80 °C during hydrolytic degradation.

hydrolysis, accompanied by the increased crystallization till Day 7, resulted in mechanically less integrated films with increased brittleness as indicated by Fig. 5S. Future research could focus on establishing a correlation between the degradation process and changes in mechanical performance. On the other hand, it indicates that after the total consumption of MAF regions (Day 26), the remained RAF and CF can still maintain the sample shape, which may be attributed to the presence of SC-crystal networking structure [48-51]. Such SC-crystal network is comprised of SC-crystal lamellas connected by the tie molecules and entangled chains, which have been found to retain their structural stability after solvent dissolution [48,49].

To understand the role of polymorphism on the above-discussed structure changes, Fig. 7 presents the evolution of HC and SC melting temperatures (A-D) and enthalpies (E-H) from Day 0 to Day 26. As previously mentioned, in general, T_{140} samples containing α + SC crystals provided HC-crystals with the greatest resistance to hydrolysis, while T_{200} samples containing exclusively SC-crystals demonstrated HC-crystal with the least hydrolytic resistance, as shown in Figs. 7A and B. At the same time, T_{80} samples with α' + SC crystals showed HC-crystals with degradation resistance comparable to those samples with initially low crystallinity exclusive SC crystals (T_{225}). However, this polymorphism-dependent degradation behavior was observed only after Day 3, once crystallization was completed. Fig. 7E-H show the evolution of HC and SC melting enthalpies from Day 0 to Day 26. On Day 3, T_{200} and T_{140} samples retained their initial HC crystallinity but achieved higher SC crystallinity due to crystallization. On the other hand, T_{225} samples attained a similar HC and SC crystallinity to T_{80} samples after Day 3. As a result, after Day 3, T_{225} samples displayed similar SC fractions to T_{80} samples, while T_{200} samples had the highest SC fraction and T_{140} samples had the lowest. This trend seems to correlate with the degradation behavior of HC-crystals, where a high SC fraction appeared to negatively influence the degradation of HC crystals, as shown in Fig. 7A and B. Hydrophilicity and hydrophobicity play a significant role in the hydrolytic degradation of PLA [52]. To evaluate the effect, the contact angle of samples from Day 0 to Day 7 with similar crystallinity but varying SC-crystal fractions were measured and shown in Fig. 6S. The contact angle measurements for films with different SC fractions (annealed at 200 °C, 140 °C, and 80 °C) before hydrolysis are comparable, indicating that the initial hydrophilicity of the samples is similar. In contrast, the hydrophilicity increased with extending hydrolysis days for all samples (lower reported water contact angle), probably due to increased surface roughness due to degradation. Therefore, surface hydrophilicity and hydrophobicity of the film might not be attributed as the significant cause of the different hydrolysis behaviors observed among those samples. On the other hand, Tsuji and coworkers previously suggested that the end groups linked to the lamellar surface might adversely affect hydrolytic resistance [11]. It is possible in the present study that more end groups were associated with SC crystals due to the involvement of two PLA chains in the unit cell of the SC-crystal. Consequently, enrichment of these end groups introduced by SC-crystals could have created autocatalytic conditions [53] conducive to the degradation of HC crystals. Furthermore, the observation that crystals and their associated RAF degraded at similar rates supports this premise, as RAF may mainly comprise amorphous chains with free ends [41], and the cleavage of these chains could be the cause of the parallel degradation of RAF and crystal.

Compared with HC-crystals, the changes in $T_{m,\,SC}$ (Fig. 7C and D) were less noticeable until Day 7 for SCPLA and Day 26 for SCPLA/LDH. This demonstrated that SC-crystals has superior resistance to hydrolysis compared to HC-crystals, which is consistent with earlier studies and can be attributed to the stronger intermolecular interaction between paired racemic helices in the unit cell of SC-crystal [17]. SC crystals in T_{140} samples with the lowest SC fraction maintained the greatest resistance to hydrolysis, suggesting that the end group that comes with the SC-crystals promoted overall degradation. However, SC-crystals in T_{200} samples, despite having the highest SC fraction, also showed high resistance. This could be due to the networking structure [48,49] of SC-crystals that might inhibit water diffusion, but further research is

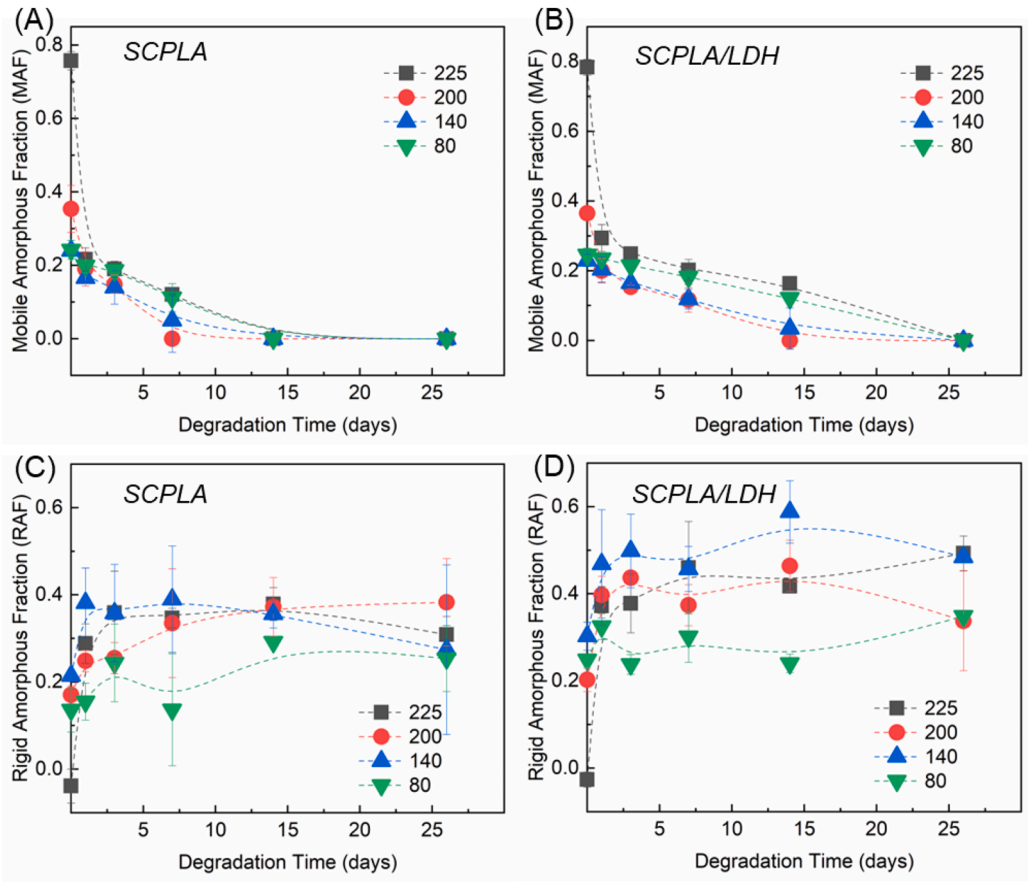

Fig. 5. Mobile amorphous fraction of (A) SCPLA and (B) SCPLA/LDH prepared from annealing at different temperatures (as marked in legend) during hydrolytic degradation. Corresponding rigid amorphous fraction of (C) SCPLA and (D) SCPLA/LDH during hydrolytic degradation.

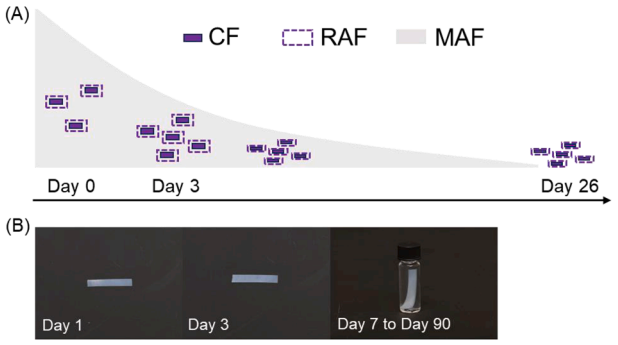

Fig. 6. (A) Schematic diagram of three-phase crystalline composition changes during hydrolytic degradation. (B) Photos of SCPLA films prepared from annealing at 225 °C during hydrolytic degradation.

needed to elucidate this mechanism. The introduction of LDH has demonstrated delays of changes in previously discussed structural parameters, indicating a protective effect of the low-content LDH against degradation. This is also evidenced by Fig. 7S, which illustrates the relative changes in the weight-average molecular weight of SCPLA and SCPLA/LDH during hydrolytic degradation in the first 14 days. Moreover, Fig. 7S shows that variations in polymorphism did not significantly affect the decrease in molecular weight. Conversely, LDH-filled composites displayed slower overall degradation than the neat SCPLA. This suggests that, in contrast to its adverse impact on thermal degradation with high-content LDH (≥1 wt%) [44,45] the lower content LDH (0.5 wt %) could have potentially inhibited the hydrolytic degradation of PLA in this study. This inhibition effect by LDH on PLA hydrolysis was reported elsewhere and attributed to the suppression of the autocatalytic degradation effect by the neutralization effect with carboxyl groups by the ionic surface of LDH [32,33,54,55]. Contrarily, at higher content of LDH (≥1 wt%), the catalyzed depolymerization effect by the Mg and Al ions of LDH [45,56] might dominate.

4. Conclusions

This work aimed to comprehend the evolution of the three-phase crystalline structure of SCPLA during hydrolytic degradation, with particular attention given to the influence of polymorphism on these processes. Degradation and crystallization occurred simultaneously during hydrolysis. Specifically, all MAFs were degraded by Day 26, degradation of CF commenced after Day 3, and crystallization was limited to the initial three days, increasing both CF and RAF fractions. The degradation rate of RAF was similar to CF, as RAF may primarily consist of amorphous chains with free ends; therefore, the degradation of these chains led to concurrent reductions in RAF and CF. Polymorphism significantly influenced the degradation behavior of the CF. Samples with a high SC fraction displayed quicker degradation of the HC-crystal, probably due to the unfavorable impact of amorphous chains with free ends associated with the SC-crystal, thereby intensifying the autocatalytic hydrolytic degradation. This phenomenon also applies to the SC-crystal degradation, except for instances where T_{200} samples with a high-to-exclusive SC fraction demonstrated remarkable resistance of SC-crystal to hydrolysis. This may be implied by the networking structure of SC-crystal inhibiting water diffusion. The introduction of LDH into SCPLA followed a similar degradation pattern as the neat SCPLA, albeit at a slower rate. This may be due to the neutralizing effect of the basic surface of LDH on the carboxyl groups which was responsible for

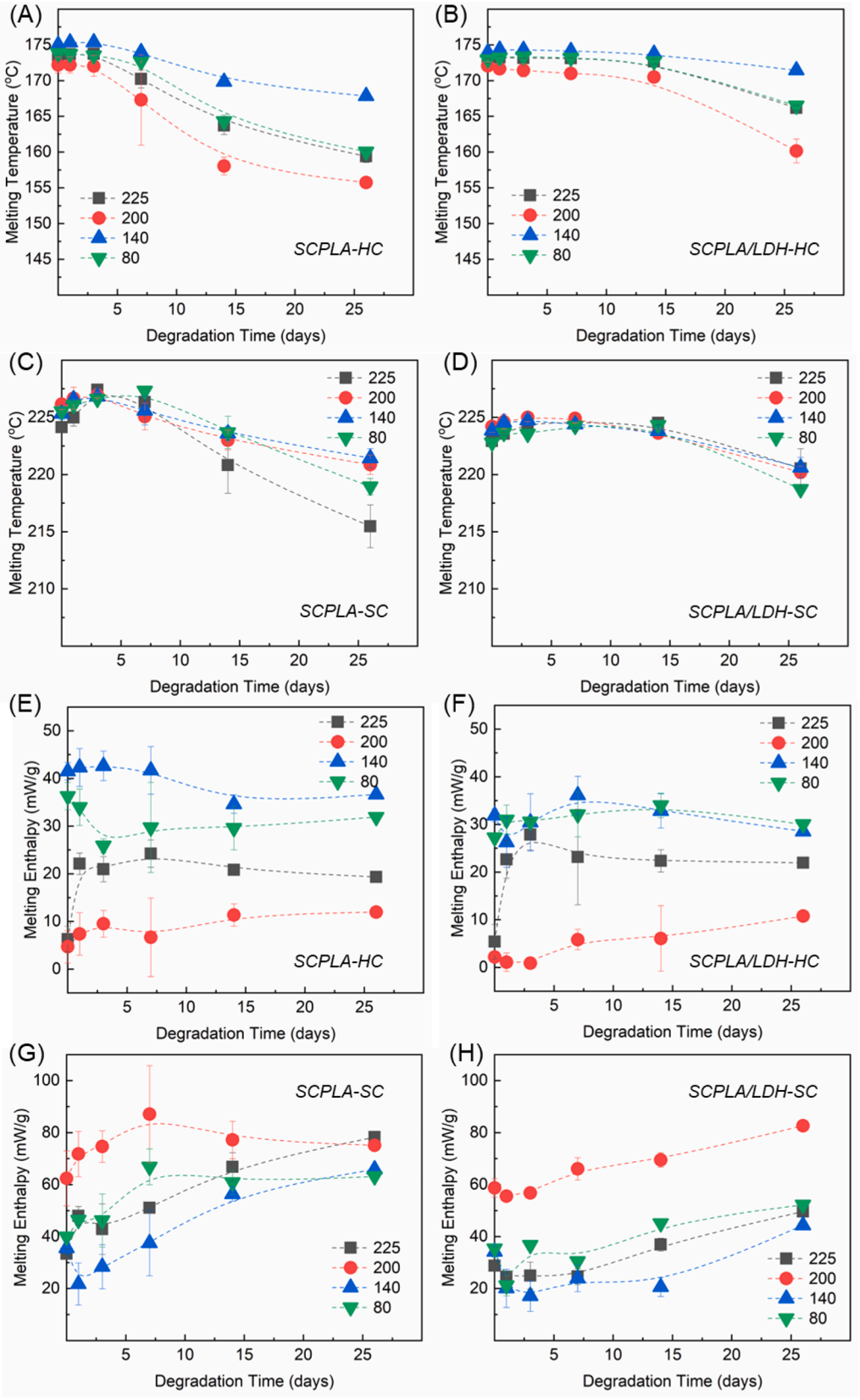

Fig. 7. (A-D) Melting temperatures of HC and SC-crystals of SCPLA and SCPLA/LDH prepared from annealing at different temperatures (as marked in legend) during hydrolytic degradation. (E-H) Melting enthalpies of HC and SC-crystals of SCPLA and SCPLA/LDH prepared from annealing at different temperatures (as marked in legend) during hydrolytic degradation.

the autocatalytic hydrolysis degradation. In conclusion, this study revealed the multi-step evolution of the three-phase crystalline structure of SCPLA during hydrolysis and the influence of SC fraction on the degradation of SC and HC crystals under hydrolytic degradation conditions. These findings could serve as a preliminary guide for future work aimed at modulating the degradation behavior of SCPLA or other semicrystalline polymers.

CRediT authorship contribution statement

Qi Chen: Conceptualization, Formal analysis, Investigation, Methodology, Validation, Visualization, Writing – original draft. **Ece Sogut:** Investigation, Methodology. **Rafael Auras:** Supervision, Writing – review & editing. **Jacob Judas Kain Kirkensgaard:** Investigation, Writing – review & editing. **Ilke Uysal-Unalan:** Conceptualization, Project administration, Resources, Supervision, Writing – review & editing, Funding acquisition, Visualization.

Declaration of competing interest

The authors declare that they have no known competing financial interests or personal relationships that could have appeared to influence the work reported in this paper.

Data availability

Data will be made available on request.

Acknowledgments

This work was supported by CiFOOD - Centre for Innovative Food Research in Aarhus University (AU). The authors would like to thank Professor Milena Corredig (Department of Food Science, AU) for her support with SEC-MALS. Data were generated through accessing research infrastructure at Aarhus University and University of Copenhagen, including FOODHAY (Food and Health Open Innovation Laboratory, Danish Roadmap for Research Infrastructure).

Supplementary materials

Supplementary material associated with this article can be found, in the online version, at doi:10.1016/j.apmt.2024.102226.

References

[1] G. Gorrasi, R. Pantani, Hydrolysis and Biodegradation of Poly (Lactic acid), Synthesis, Structure and Properties of Poly (Lactic acid), 2018, pp. 119–151.
[2] H. Tsuji, Hydrolytic degradation, Poly (Lactic Acid) Synthesis, Structures, Properties, Processing, Applications, and End of Life, 2022, pp. 467–516.
[3] O. Avinc, M. Wilding, D. Phillips, D. Farrington, Investigation of the influence of different commercial softeners on the stability of poly(lactic acid) fabrics during storage, Polym. Degrad. Stab. 95 (2) (2010) 214–224.
[4] V. Taubner, R. Shishoo, Influence of processing parameters on the degradation of poly(L-lactide) during extrusion, J. Appl. Polym. Sci. 79 (12) (2001) 2128–2135.
[5] R. Auras, B. Harte, S. Selke, An overview of polylactides as packaging materials, Macromol. Biosci. 4 (9) (2004) 835–864.
[6] B.-Y. Su, Z.-J. Chen, J.-C. Lv, Z.-G. Wang, F.-W. Huang, Y. Liu, E. Luo, J. Wang, J.-Z. Xu, Z.-M. Li, Scalable fabrication of polymeric composite microspheres to inhibit oral pathogens and promote osteogenic differentiation of periodontal membrane stem cells, ACS Biomater. Sci. Eng. 9 (7) (2023) 4431–4441.
[7] M.A. Elsawy, K.-H. Kim, J.-W. Park, A. Deep, Hydrolytic degradation of polylactic acid (PLA) and its composites, Renew. Sustain. Energy Rev. 79 (2017) 1346–1352.
[8] H. Tsuji, S. Miyauchi, Poly(l-lactide): VI Effects of crystallinity on enzymatic hydrolysis of poly(l-lactide) without free amorphous region, Polym. Degrad. Stab. 71 (3) (2001) 415–424.
[9] N. Zhang, X. Yu, J. Duan, J.-h. Yang, T. Huang, X.-d. Qi, Y. Wang, Comparison study of hydrolytic degradation behaviors between α′- and α-poly(l-lactide), Polym. Degrad. Stab. 148 (2018) 1–9.
[10] H. Tsuji, Y. Ikada, Properties and morphology of poly(l-lactide) 4. Effects of structural parameters on long-term hydrolysis of poly(l-lactide) in phosphate-buffered solution, Polym. Degrad. Stab. 67 (1) (2000) 179–189.
[11] H. Tsuji, A. Mizuno, Y. Ikada, Properties and morphology of poly(L-lactide). III. Effects of initial crystallinity on long-term in vitro hydrolysis of high molecular weight poly(L-lactide) film in phosphate-buffered solution, J. Appl. Polym. Sci. 77 (7) (2000) 1452–1464.
[12] H. Tsuji, C.A. Del Carpio, In Vitro hydrolysis of blends from enantiomeric Poly (lactide)s. 3. Homocrystallized and amorphous blend films, Biomacromolecules. 4 (1) (2003) 7–11.
[13] Q. Chen, R. Auras, I. Uysal-Unalan, Role of stereocomplex in advancing mass transport and thermomechanical properties of polylactide, Green Chem. 24 (9) (2022) 3416–3432.
[14] Y. Li, Z.-Z. Shi, L. Bai, R.-Y. Bao, M.-B. Yang, W. Yang, Enhanced polylactide stereocomplexes by aluminum oxide particles for reliable thermal conductivity at elevated temperature, Polymer. (Guildf) 270 (2023) 125775.
[15] J.-Z. Xu, Y. Li, Y.-K. Li, Y.-W. Chen, R. Wang, G. Liu, S.-M. Liu, H.-W. Ni, Z.-M. Li, Shear-induced stereocomplex cylindrites in polylactic acid racemic blends: morphology control and interfacial performance, Polymer. (Guildf) 140 (2018) 179–187.
[16] Y.-Y. Liang, J.-Z. Xu, Y. Li, G.-J. Zhong, R. Wang, Z.-M. Li, Promoting interfacial Transcrystallization in Polylactide/Ramie fiber composites by utilizing Stereocomplex crystals, ACS Sustain. Chem. Eng. 5 (8) (2017) 7128–7136.
[17] H. Tsuji, T. Tsuruno, Accelerated hydrolytic degradation of Poly(l-lactide)/Poly(d-lactide) stereocomplex up to late stage, Polym. Degrad. Stab. 95 (4) (2010) 477–484.
[18] H. Tsuji, Poly(lactic acid) stereocomplexes: a decade of progress, Adv. Drug Deliv. Rev. 107 (2016) 97–135.
[19] H. Tsuji, In vitro hydrolysis of blends from enantiomeric poly(lactide)s Part 1. Well-stereo-complexed blend and non-blended films, Polymer. (Guildf) 41 (10) (2000) 3621–3630.
[20] H. Tsuji, In vitro hydrolysis of blends from enantiomeric poly (lactide) s. Part 4: well-homo-crystallized blend and nonblended films, Biomaterials 24 (4) (2003) 537–547.
[21] M.L. Di Lorenzo, M.C. Righetti, Crystallization-induced formation of rigid amorphous fraction, Polymer Crystallizat. 1 (2) (2018) e10023.
[22] H. Suzuki, J. Grebowicz, B. Wunderlich, Glass transition of poly(oxymethylene), Brit. Polym. J. 17 (1) (1985) 1–3.
[23] B. Wunderlich, Reversible crystallization and the rigid–amorphous phase in semicrystalline macromolecules, Prog. Polym. Sci. 28 (3) (2003) 383–450.
[24] W. Limsukon, R. Auras, T. Smith, Effects of the three-phase crystallization behavior on the hydrolysis of amorphous and semicrystalline Poly(lactic acid)s, ACS Appl. Polym. Mater. 3 (11) (2021) 5920–5931.
[25] S. Wietzke, C. Jansen, M. Reuter, T. Jung, J. Hehl, D. Kraft, S. Chatterjee, A. Greiner, M. Koch, Thermomorphological study of the terahertz lattice modes in polyvinylidene fluoride and high-density polyethylene, Appl. Phys. Lett. 97 (2) (2010).
[26] J. Lin, S. Shenogin, S. Nazarenko, Oxygen solubility and specific volume of rigid amorphous fraction in semicrystalline poly(ethylene terephthalate), Polymer. (Guildf) 43 (17) (2002) 4733–4743.
[27] A. Guinault, C. Sollogoub, V. Ducruet, S. Domenek, Impact of crystallinity of poly (lactide) on helium and oxygen barrier properties, Eur. Polym. J. 48 (4) (2012) 779–788.
[28] M. Drieskens, R. Peeters, J. Mullens, D. Franco, P.J. Lemstra, D.G. Hristova-Bogaerds, Structure versus properties relationship of poly(lactic acid). I. Effect of crystallinity on barrier properties, J. Polym. Sci. Part B: Polym. Phys. 47 (22) (2009) 2247–2258.
[29] F. Codari, S. Lazzari, M. Soos, G. Storti, M. Morbidelli, D. Moscatelli, Kinetics of the hydrolytic degradation of poly(lactic acid), Polym. Degrad. Stab. 97 (11) (2012) 2460–2466.
[30] Q. Chen, R. Auras, M. Corredig, J.J.K. Kirkensgaard, A. Mamakhel, I. Uysal-Unalan, New opportunities for sustainable bioplastic development: tailorable polymorphic and three-phase crystallization of stereocomplex polylactide by layered double hydroxide, Int. J. Biol. Macromol. 222 (2022) 1101–1109.
[31] T.T. Hu, Z. Gu, G.R. Williams, M. Strimaite, J.J. Zha, Z. Zhou, X.C. Zhang, C.L. Tan, R.Z. Liang, Layered double hydroxide-based nanomaterials for biomedical applications, Chem. Soc. Rev. 51 (14) (2022) 6126–6176.
[32] A. Oyarzabal, A. Mugica, A.J. Müller, M. Zubitur, Hydrolytic degradation of nanocomposites based on poly(l-lactic acid) and layered double hydroxides modified with a model drug, J. Appl. Polym. Sci. 133 (28) (2016).
[33] V. Iozzino, H. Askanian, F. Leroux, V. Verney, R. Pantani, Poly (lactic acid)-based nanobiocomposites with modulated degradation rates, Materials. (Basel) 11 (10) (2018) 1943.
[34] Q. Chen, R. Auras, J.J.K. Kirkensgaard, I. Uysal-Unalan, Modulating barrier properties of Stereocomplex polylactide: the polymorphism mechanism and its relationship with rigid amorphous fraction, ACS Appl. Mater. Interfaces 15 (42) (2023) 49678–49688.
[35] ASTM, ASTM D4754–18. Standard Test Method for Two-Sided Liquid Extraction of Plastic Materials Using FDA Migration Cell, ASTM, 2018.
[36] K. Wasanasuk, K. Tashiro, Crystal structure and disorder in Poly(l-lactic acid) δ form (α′ form) and the phase transition mechanism to the ordered α form, Polymer. (Guildf) 52 (26) (2011) 6097–6109.
[37] J. Zhang, K. Tashiro, H. Tsuji, A.J. Domb, Disorder-to-order phase transition and multiple melting behavior of Poly(l-lactide) investigated by simultaneous measurements of WAXD and DSC, Macromolecules. 41 (4) (2008) 1352–1357.
[38] M.L. Di Lorenzo, R. Androsch, Influence of α′-/α-crystal polymorphism on properties of poly(l-lactic acid), Polym. Int. 68 (3) (2019) 320–334.

[39] L. Aliotta, P. Cinelli, M.B. Coltelli, M.C. Righetti, M. Gazzano, A. Lazzeri, Effect of nucleating agents on crystallinity and properties of poly (lactic acid) (PLA), Eur. Polym. J. 93 (2017) 822–832.
[40] S.K. Saha, H. Tsuji, Effects of molecular weight and small amounts of D-lactide units on hydrolytic degradation of poly(l-lactic acid)s, Polym. Degrad. Stab. 91 (8) (2006) 1665–1673.
[41] H. Tsuji, K. Ikarashi, In Vitro hydrolysis of Poly(l-lactide) crystalline residues as extended-chain crystallites: II. Effects of hydrolysis temperature, Biomacromolecules. 5 (3) (2004) 1021–1028.
[42] X. Zhang, M. Espiritu, A. Bilyk, L. Kurniawan, Morphological behaviour of poly (lactic acid) during hydrolytic degradation, Polym. Degrad. Stab. 93 (10) (2008) 1964–1970.
[43] M.-F. Chiang, M.-Z. Chu, T.-M. Wu, Effect of layered double hydroxides on the thermal degradation behavior of biodegradable poly(l-lactide) nanocomposites, Polym. Degrad. Stab. 96 (1) (2011) 60–66.
[44] N. Delpouve, A. Saiter-Fourcin, S. Coiai, F. Cicogna, R. Spiniello, W. Oberhauser, S. Legnaioli, R. Ishak, E. Passaglia, Effects of organo-LDH dispersion on thermal stability, crystallinity and mechanical features of PLA, Polymer. (Guildf) 208 (2020) 122952.
[45] J. Leng, N. Kang, D.-Y. Wang, J. Falkenhagen, A.F. Thünemann, A. Schönhals, Structure–property relationships of nanocomposites based on polylactide and layered double hydroxides – comparison of MgAl and NiAl LDH as NANOFILLER, Macromol. Chem. Phys. 218 (20) (2017) 1700232.
[46] F.v. Burkersroda, L. Schedl, A. Göpferich, Why degradable polymers undergo surface erosion or bulk erosion, Biomaterials 23 (21) (2002) 4221–4231.
[47] F. Iñiguez-Franco, R. Auras, J. Ahmed, S. Selke, M. Rubino, K. Dolan, H. Soto-Valdez, Control of hydrolytic degradation of Poly(lactic acid) by incorporation of chain extender: from bulk to surface erosion, Polym. Test. 67 (2018) 190–196.
[48] X.-F. Wei, R.-Y. Bao, Z.-Q. Cao, W. Yang, B.-H. Xie, M.-B. Yang, Stereocomplex crystallite network in asymmetric PLLA/PDLA blends: formation, structure, and confining effect on the crystallization rate of homocrystallites, Macromolecules. 47 (4) (2014) 1439–1448.
[49] J. Wang, R. Lv, B. Wang, B. Na, H. Liu, Direct observation of a stereocomplex crystallite network in the asymmetric polylactide enantiomeric blends, Polymer. (Guildf) 143 (2018) 52–57.
[50] S. Saeidlou, M.A. Huneault, H. Li, P. Sammut, C.B. Park, Evidence of a dual network/spherulitic crystalline morphology in PLA stereocomplexes, Polymer. (Guildf) 53 (25) (2012) 5816–5824.
[51] Z. Jing, X. Shi, G. Zhang, J. Li, J. Li, L. Zhou, H. Zhang, Formation, structure and promoting crystallization capacity of stereocomplex crystallite network in the poly (lactide) blends based on linear PLLA and PDLA with different structures, Polymer. (Guildf) 92 (2016) 210–221.
[52] M.A. Paul, C. Delcourt, M. Alexandre, P. Degée, F. Monteverde, P. Dubois, Polylactide/montmorillonite nanocomposites: study of the hydrolytic degradation, Polym. Degrad. Stab. 87 (3) (2005) 535–542.
[53] H. Tsuji, Autocatalytic hydrolysis of amorphous-made polylactides: effects of L-lactide content, tacticity, and enantiomeric polymer blending, Polymer. (Guildf) 43 (6) (2002) 1789–1796.
[54] Q. Zhou, M. Xanthos, Nanoclay and crystallinity effects on the hydrolytic degradation of polylactides, Polym. Degrad. Stab. 93 (8) (2008) 1450–1459.
[55] Q. Zhou, M. Xanthos, Effects of cationic and anionic clays on the hydrolytic degradation of polylactides, Polym. Eng. Sci. 50 (2) (2010) 320–330.
[56] J. Leng, P.J. Purohit, N. Kang, D.-Y. Wang, J. Falkenhagen, F. Emmerling, A. F. Thünemann, A. Schönhals, Structure–property relationships of nanocomposites based on polylactide and MgAl layered double hydroxides, Eur. Polym. J. 68 (2015) 338–354.